Disturbance, Management, and Landscape Dynamics: Harmonic Regression of Vegetation Indices in the Lower Okavango Delta, Botswana

Amy L. Neuenschwander and Kelley A. Crews

Abstract

Focused on the Okavango Delta, Botswana, this research investigates (a) whether ecosystem signals derived from remotely sensed imagery can be decomposed using a harmonic regression, (b) if the deviations from the decomposed signal are correlated with observed flooding and fire regimes, and (c) the impact of explicitly including agriculture, settlement areas, and land management systems on the derived signals. A time-series of 85 TM/ETM+ *scenes spanning the period from 1989 through 2002 was used to decompose derived landscape dynamics into trends, annual and seasonal cycles, and long term oscillations. The harmonic fit largely defined by climatic periodicities (semi-annual, annual, and quasi-decadal) accounted for 63 percent to 88 percent of the variance in the trajectories. The trends were found to be robust whether or not urban settlement or landscape management regimes were explicitly included, though there was a reversal of trend in agricultural areas.*

Introduction

The objective of this research was to utilize remotely sensed imagery to quantify the impact of flooding, fire, and their interaction as derived through vegetation response over time in the Okavango Delta. The Okavango Delta system, located in northern Botswana, is experiencing both human-induced and natural changes at a variety of spatio-temporal scales (McCarthy *et al.*, 2000). One method of examining the dynamics of a system is through the analysis of ecological time-series data (Rodriquez-Trelles *et al.*, 1996; West, 1997). This research investigates whether ecosystem signals derived from remotely sensed imagery can be decomposed with harmonic regression and wavelets, and if the deviations from the decomposed signal are correlated with observed flooding and fire regimes. Specifically, the motivation behind decomposing the signal is to identify trends and cycles observed in the vegetation dynamics related to climatic or anthropogenic forces. Further, this paper aims to understand the correlation of these trends and cycles with different drivers of landscape change (in particular climate and anthropogenic pressures) on the vegetation behavior as observed using a vegetation index derived from remotely sensed imagery. That is, can the impacts of anthropogenic pressures be disentangled from natural pressures by examining periodicities in Enhanced Vegetation Index calculations? Temporal analysis of ecosystem trajectories has been reported as successfully decomposed into two general categories: permanent and transitory signals (Rodriguez-Arias and Rodo, 2004). Permanent signals are composed of trends, seasonal and annual cycles, long term cycles, and structured residuals (Jassby and Powell, 1990). Transitory signals, in contrast, are signals that are temporary and discrete within a time series, such as from a disturbance (Rodriguez-Arias and Rodo, 2004). Disentangling these two types of signal is critical for better assessing the interrelationships among climatic oscillations, disturbance regimes, human management, and ecosystem response (Lundberg *et al.*, 2000).

Given these oscillations, disturbances, and distance regimes, this research is in large part motivated by the theory of ecosystem resilience. This concept emerged during the 1970s as both theoretical and applied ecologists began to realize that models predicated on concepts of ecological equilibrium were often inappropriate for accurately depicting complex, real-world data (Holling, 1973; DeAngelis and Waterhouse, 1987). Ecosystem resilience centers on the magnitude of disturbance that an ecosystem can sustain without shifting into an alternate state (Folke *et al.*, 2004). Since resilience is a property that cannot be directly measured or quantified, the development of indicators and critical thresholds is necessary to monitor ecosystem resiliency or stability. For many of the resilience indicators suggested (Bennett *et al.*, 2005), knowledge of ecosystem feedbacks is necessary so that a threshold can be employed. However, in complex systems (e.g., savanna) with several variables acting upon that system (fire, elephants, woodland/grassland competition) resulting in complex feedback loops, thresholds can fluctuate or can be difficult to determine. For these types of systems, Bennett *et al.* (2005) suggest that the rate of change and the direction of that change in key variables can be used as a resilience indicator. Here the variable utilized is vegetation response as derived from Enhanced Vegetation Index (EVI) values. EVI has been documented as a

Department of Geography & the Environment and the Center for Space Research, University of Texas at Austin, Austin, TX 78712 (kacm@uts.cc.utexas.edu).

Photogrammetric Engineering & Remote Sensing
Vol. 74, No. 6, June 2008, pp. 000–000.

0099-1112/08/7406–0000/$3.00/0

more robust vegetation index than NDVI for assessing seasonality of ecological processes in a grassland-shrubland-woodland matrix (Ferreira *et al.*, 2003). This type of monitoring is offered as an alternative to traditional post-classification change detection, allowing for quicker calculation over time-series with frequent observations, and that detects subtle shifts within classes (e.g., changing vegetation density within a savanna cover class).

Site and Situation

The Okavango Delta provides critical habitat and resources to humans and wildlife (including large and endangered mammal populations), and for this reason has been internationally recognized as a wetland of importance by the Ramsar Convention on Wetlands (Kgathi *et al.*, 2005). However, changes in land-use, such as the extraction of resources (water, fish, wood, and reeds), increased burning, overgrazing of domestic livestock, and a growing tourism industry, threaten this wetland-savanna environment (Mbaiwa *et al.*, 2002; Kgathi *et al.*, 2006). Further, the recent return of Angolan refugees to the Delta's sourcewater region and concomitant proposed water diversion for consumptive sanitation and irrigation purposes threatens the relatively undocumented baseline function of this fragile ecosystem (Andersson *et al.*, 2003; Ashton, 2003).

Humans are additionally influencing the functioning of the Delta through burning, both for hunting purposes and the clearing of vegetation. The area's vegetation is also affected by two major disturbance regimes, flooding and fire, but is also influenced by grazing, browsing, human activity, and shifting climatic conditions. The study area is located in the distal region of the Delta near Maun at the wetland/savanna interface and is approximately 2,430 km^2 in size (see Figure 1). The vegetation within the study area varies considerably and includes sedges/reeds and grasses found in the channels and floodplains, Acacia dominated savannas of various densities of tree cover in the drylands, woodlands dominated by Mopane, Combretum, and Acacia, and riparian forest located on the fringe of many small islands within the wetlands.

The annual flooding in the Okavango Delta sustains the wetland system which in turn provides valuable resources for the people and wildlife occupying this semi-arid region of northern Botswana. The distribution of floodwaters across the broad alluvial fan is dependent upon several factors, including the total inflow to the system originating upstream of the Okavango River, the amount of localized rainfall over the fan, the growth of vegetation within the channels that blocks and diverts the flow of water, and presence of large animals (particularly hippopotamus) to open new channels (McCarthy *et al.*, 1998; Ellery *et al.*, 2003). The temporal variability of the localized precipitation from year to year is reported to follow 3-, 8-, and 18-year precipitation cycles common to southern Africa (Tyson *et al.*, 2002) with the largest oscillation occurring at the 18-year interval (McCarthy *et al.*, 2000).

Methodology

To conduct this analysis, a time-series of 85 TM/ETM+ scenes ranging from April 1989 through October 2002 ~~were~~ ^ used, where images were spaced roughly every two to three months. Previously, this time-series was used to extract the spatial and temporal distribution of the flooding and fire regimes and their interaction in the Okavango Delta (Heinl *et al.*, 2006). Patterns of flooding and fire from individual scenes were combined to create annual flooding and fire extent maps (Plate 1). A majority of the fires were found to occur within the floodplains (Neuenschwander and Crews-Meyer, 2006) and the extracted disturbance maps were used as a comparison for the vegetation assessment derived from the imagery. A flowchart of the methodological steps used in this analysis is shown in Figure 2 and is followed in the

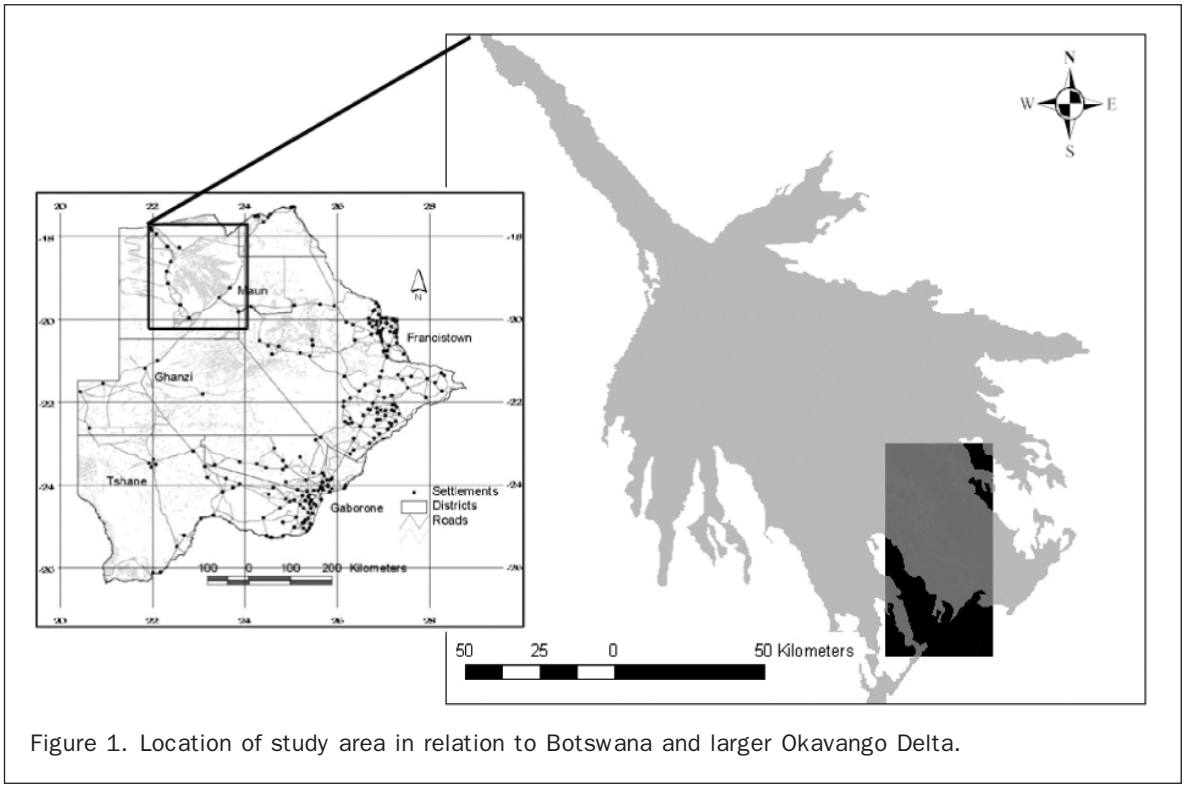

Figure 1. Location of study area in relation to Botswana and larger Okavango Delta.

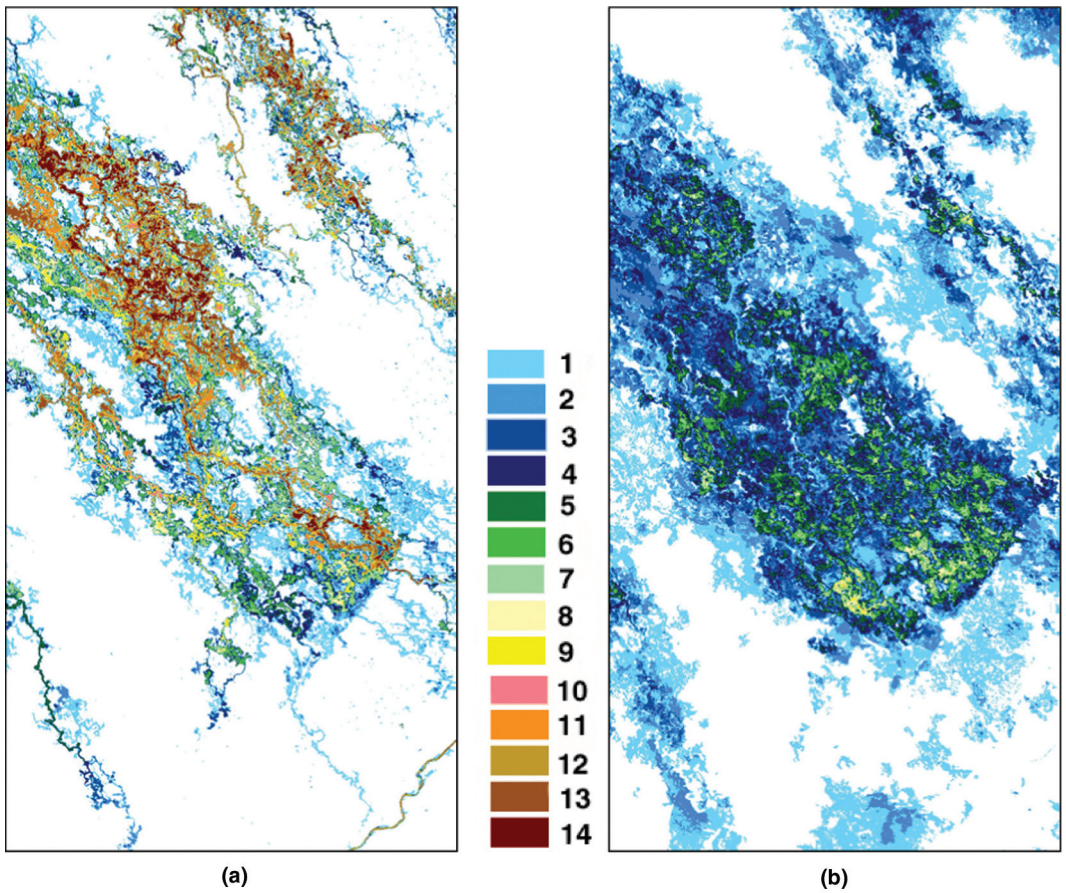

Plate 1. Fourteen-year history in the lower Okavango Delta, Botswana of (a) Flooding, and (b) fire. The legend is the same for both maps and represents the number of years in the 14-year time-series where either flooding or fire occurred.

discussion below of the order of processing steps: (a) preprocessing, (b) calculation of mean EVI trajectories, (c) harmonic regression and wavelet analysis, and (d) stratification of results using land management and urban/agricultural areas.

Preprocessing and Mean EVI Trajectory Creation

Each of the 85 TM/ETM+ scenes was converted into both apparent top of atmosphere (TOA) reflectance (by adjusting for solar angle) and effective surface reflectance (by adjusting for solar angle and correcting for atmospheric scattering using Dark Object Subtraction, or DOS) (Chavez, 1988; Chavez and MacKinnon, 1994). Landscape trajectories were found to exhibit different patterns and trends when using TOA reflectance instead of atmospherically corrected reflectance, revealing the importance of atmospheric and radiometric correction in multi-temporal studies. The DOS-corrected dataset produced the more consistent spectral response through the time-series, and thus subsequent results presented in this paper were implemented on the DOS-corrected dataset (Song *et al.*, 2001; Schroeder *et al.*, 2006). The Enhanced Vegetation Index (EVI) was selected for use in this research as it is a widely used and accepted indicator of vegetation vigor and minimizes some of the weakness common with NDVI (Huete *et al.*, 2002). Importantly, EVI has been reported to be more sensitive (a) to weak vegetation signals in semi-arid savannas by minimizing the soil background (Huete *et al.*, 1997), and (b) to variations in canopy structure (Gao *et al.*, 2000). In particular, EVI has been found to be negatively associated with woody cover and positively associated with herbaceous vegetation (Fang *et al.*, 2005).

EVI images were calculated for each scene individually, and then stacked into a time-series such that each pixel had an 85-member trajectory of EVI. In order to group pixels that exhibited similar trajectories in EVI change through time, an ISODATA clustering algorithm was run on the 85-layer file, where each EVI image at a given date is analogous to a spectral band. Thus, the output product from this clustering represents regions on the landscape that are temporally statistically similar, rather than spectrally similar as with standard ISODATA applications (Crews-Meyer, 2002). Thirty-five output clusters were selected based upon spectral and information classes previously identified in landcover mapping studies of the area (12 classes in McCarthy *et al.*, 2006; 23 classes in Neuenschwander *et al.*, 2006); both a drop and threshold in class separability supported the cutoff at 35 classes, yielding a manageable and interpretable set of classes and results. This output of the ISODATA results was next used as a spatial mask to map each of the 35 temporal clusters into individual images for further analysis. Then, the mean EVI value for each of the 35 cluster-images was calculated based upon the values in each pixel's trajectory. Thus, the mean behavior of the vegetation response from 1989 through 2002 as represented by EVI was described as

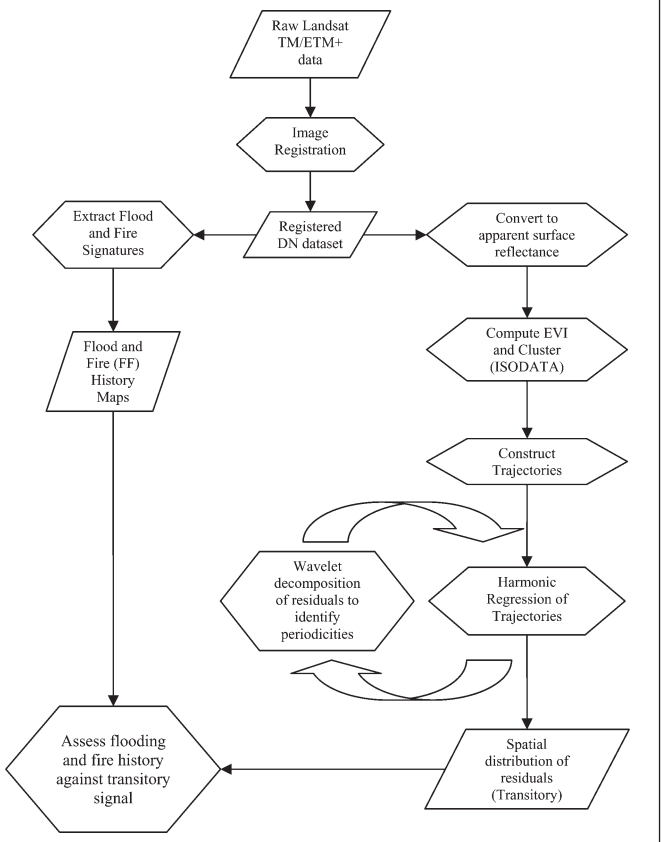

Figure 2. Flowchart of processing steps.

an 85 element vector, and mapped separately for each of the 35 temporal clusters. Additionally, the flooding and fire histories for each EVI cluster were computed from previous mapping efforts (Heinl *et al.*, 2006), resulting in an 85 element trajectory of flooding or fire. Here, the frequency of pixels through time having been classified as either flooding or fire was used to generate both flooding and fire trajectories for each of the 35 temporal clusters.

Harmonic Regression, Wavelet Analysis, and Landscape Management Stratification

Harmonic regression is less typically employed by the landscape remote sensing community for detecting land-use or land-cover change using optical imagery, though it has been utilized in studies centering on climate change and global vegetation cycles (Braswell *et al.*, 1997) and/or when sufficiently rich time-series are available, such as with MODIS data (Bradley *et al.*, 2007). Rather than fitting the data to a linear or polynomial function, harmonic regression fits data to a described trend and cycle using a sine wave. The harmonic regression model used in this research takes the form:

$$y = \beta_0 + cT + \sum_{i=1}^{m} A_i \sin\left(\frac{2\pi i}{s}T + \phi_i\right)$$

where y is EVI, β_0 is an offset, c is the trend, A_i is the amplitude of the i^{th} oscillation, ϕ_i is the phase component of the i^{th} oscillation, s is the fundamental frequency (in this case, one year), and T is the dependent time variable. The motivation for implementing a harmonic regression in this research is to quantitatively describe the trends and patterns of land-cover trajectories hypothesized to correspond to cyclical events or processes. A harmonic regression of the mean EVI trajectory was fit against time for each EVI-based trajectory to determine general trends and to reveal the temporal patterns for each EVI cluster. First, a bias, trend, semi-annual (six-month) and annual cycle were fit to the data. An annual cycle is modeled to account for the annual variability in the signal. Similarly, because the Okavango Delta is located within the subtropics and has distinct wet and dry seasons each year, a semi-annual cycle was included to represent the distinct wet/dry seasonality of the region. Because climatic patterns are cyclical, a Morlet wavelet was run on each EVI-residual trajectory. The Morlet wavelet is a continuous wavelet based upon a sine wave and multiplied by a Gaussian function, whose resulting sinusoidal shape makes it appropriate for use with data hypothesized to have a cyclical component.

As noted earlier, ecological time-series data may consist of longer term signals in addition to the seasonal signals. For each EVI-based trajectory, the residuals from the semi-annual and annual fit were extracted and subsequently examined to identify any additional cycles beyond an annual pattern. However, the periodicity of the remaining signals is not known; therefore a wavelet analysis was used after the harmonic regression to identify possible longer terms cycles. Wavelet analysis has been widely used in many fields including geophysics, ecological studies (Saunders *et al.*, 2004; Mi *et al.*, 2005), hydrology (Labat *et al.*, 2004) and climate studies (Kestin *et al.*, 1998) for characterizing temporal and frequency variability in time series data. Wavelets decompose the input signal into a set of dominant frequencies and then determine when the variability fluctuations occur in time (Torrence and Compo, 1998; Kestin *et al.*, 1998). Due to the uneven temporal spacing of the original time-series, the EVI-based trajectories were linearly interpolated into equal 15.5-day intervals for the subsequent wavelet analysis. The resulting residual trajectories were then compared to flooding and fire histories and also geographically stratified by the four primary management zones (reserve, hunting concession, photography concession, and open use/communal) as well as by the presence of agriculture/urban settlements.

Results and Discussion

Harmonic Regression and Wavelet Analysis

In the first iteration of our analysis, we fitted the EVI time series for each temporal cluster with trend, bias, annual- and semi-annual-cycle terms. The T-test and 2-tailed significance of each model coefficient (i.e., trend, semi-annual, and annual terms) for each EVI cluster are listed in Table 1. The annual cycle was statistically significant for all EVI clusters. The semi-annual cycle was statistically significant for all but four EVI clusters and those four EVI clusters are located in the Boro River floodplain. However, the analysis of residuals revealed an additional period for inclusion in the model. Because climatic patterns, and therefore the residuals, are cyclical, a Morlet wavelet was run on each EVI-residual trajectory (Table 2). The motivation behind using the wavelet analysis was to identify any remaining cycles within each residual signal. In each of the residual trajectories, an annual pattern was found to exist, superimposed on a longer-term curve. As an illustration, the wavelet power spectrum and global wavelet for the residual trajectory of EVI-cluster 2 are shown in Figure 3. The wavelet power spectrum is a plot of the variability of multiple frequencies detected in the time series plotted against time. The global

Table 1. Two-tailed T-Test and Significance of Each Model Coefficient Term for All 35 evi Clusters. ~~Significant Coefficients are Highlighted in Grey~~

EVI Cluster	Semi-Annual T-test	*p*	Annual T-test	*p*
1	1.93E + 00	0.0286	15.34	<0.0001
2	−1.55E + 00	0.0614	10.70	<0.0001
3	−1.56E + 00	0.0614	9.81	<0.0001
4	9.45E − 01	0.1738	10.48	<0.0001
5	2.25E + 00	0.0137	14.36	<0.0001
6	2.29E + 00	0.0124	19.68	<0.0001
7	1.75E + 00	0.0421	14.38	<0.0001
8	3.27E + 00	0.0008	11.77	<0.0001
9	2.78E + 00	0.0034	13.95	<0.0001
10	−3.43E + 00	0.0005	12.15	<0.0001
11	−4.20E + 00	<0.0001	14.94	<0.0001
12	6.32E + 00	<0.0001	17.74	<0.0001
13	−4.24E + 00	<0.0001	12.57	<0.0001
14	5.21E + 00	<0.0001	17.62	<0.0001
15	5.22E + 00	<0.0001	12.09	<0.0001
16	4.25E + 00	<0.0001	12.69	<0.0001
17	5.28E + 00	<0.0001	14.39	<0.0001
18	4.48E + 00	<0.0001	14.14	<0.0001
19	6.20E + 00	<0.0001	17.30	<0.0001
20	−6.22E − 03	<0.0001	16.34	<0.0001
21	−3.32E + 00	0.0009	14.16	<0.0001
22	−4.28E + 00	<0.0001	17.29	<0.0001
23	4.90E + 00	<0.0001	16.62	<0.0001
24	−4.52E + 00	<0.0001	17.00	<0.0001
25	2.63E + 00	0.0052	13.97	<0.0001
26	−4.10E + 00	<0.0001	15.30	<0.0001
27	−4.14E + 00	<0.0001	15.25	<0.0001
28	−4.07E + 00	<0.0001	13.96	<0.0001
29	3.93E + 00	0.0001	18.33	<0.0001
30	−5.01E + 00	<0.0001	16.18	<0.0001
31	5.00E + 00	<0.0001	14.61	<0.0001
32	−3.59E + 00	0.0003	14.98	<0.0001
33	1.36E + 00	0.0889	13.48	<0.0001
34	−4.05E + 00	<0.0001	17.70	<0.0001
35	−3.85E + 00	0.0001	18.81	<0.0001

Table 2. Dominant Periodicities in Years of evi-residual Trajectories as Determined Using Wavelet Analysis. A 10.9-year Frequency was Found to be the Dominant Frequency for All but Six of the evi Clusters

EVI cluster	~~MAX~~ ^	ALL Frequencies (years)				
1	0.8	0.8	2.8	10.9	**	**
2	1.0	1.0	2.6	5.1	10.9	**
3	10.9	0.9	1.8	5.3	10.9	**
4	2.6	0.9	2.6	**	**	**
5	10.9	0.9	1.6	2.7	10.9	**
6	10.9	1.0	1.6	10.9	**	**
7	10.9	1.0	1.5	3.9	10.9	**
8	2.5	2.5	4.9	**	**	**
9	10.9	1.0	1.5	10.9	**	**
10	10.9	2.4	4.9	10.9	**	**
11	1.7	0.7	1.7	4.4	10.9	**
12	5.9	0.6	1.3	2.7	5.9	11.3
13	10.9	0.7	1.5	5.5	10.9	**
14	10.9	0.6	1.4	2.3	10.9	**
15	10.9	1.1	2.3	5.9	10.9	**
16	10.9	0.6	1.6	5.3	10.9	**
17	10.9	0.4	1.5	2.8	10.9	**
18	10.9	0.6	1.4	2.6	10.9	**
19	10.9	0.6	1.5	10.9	**	**
20	10.9	0.6	1.5	4.9	10.9	**
21	10.9	1.0	1.7	5.3	10.9	**
22	10.9	0.7	1.6	3.7	5.3	10.9
23	10.9	0.6	1.5	10.9	**	**
24	10.9	1.6	3.3	5.5	10.9	**
25	10.9	1.6	10.9	**	**	**
26	10.9	1.6	3.0	10.9	**	**
27	10.9	1.6	3.3	10.9	**	**
28	10.9	0.7	1.5	2.8	10.9	**
29	10.9	0.7	1.6	10.9	**	**
30	10.9	0.6	1.6	10.9	**	**
31	10.9	0.6	1.5	6.1	10.9	**
32	10.9	1.0	1.7	5.5	10.9	**
33	10.9	1.5	3.9	10.9	**	**
34	10.9	0.7	1.6	10.9	**	**
35	10.9	1.0	1.7	10.9	**	**

wavelet is the time averaged wavelet spectrum over all wavelet scales and it is roughly equivalent to a Fourier transform. Here, the dominant frequency in the residual signal as determined by the maximum power is at the one-year cycle. Although an annual signal was removed, the one-year cycle in the residual signal is an indication of the variability to the annual signal. Thus, it is still apparent in the residual signal. In all but six of the EVI-residual trajectories, a quasi-decadal signal (10.9 years) was detected as the frequency having the dominant power from the wavelet analysis results. Because the length of this time-series is only 14 years, the detection of a 10.9 year cycle is not statistically significant. However, there are additional observations of a quasi-decadal cycle in hydrography data that provide empirical evidence of its presence, discussed further below.

Of the six trajectories where the quasi-decadal signal was not the dominant signal, two had a dominant frequency of one year, one had a dominant frequency of 1.7 years, two had a dominant frequency of 2.5 years, and one had a dominant frequency of 5.9 years and they are spatially presented in Figure 4. Clusters having a dominant frequency of one year were found to be associated with high levels of flooding (flooding approximately every year) and frequent burning (burning every one to two years), whereas the dominant 1.7-year residuals were associated with intermediate levels of burning (burning every three to four years) and no flooding. Similarly, clusters having the 2.5-year and 5.9-year dominant residual frequency were associated with low to intermediate amounts of burning (two to four times in the 14-year time-series) and flooding approximately every other year. The fact that the dominant residual frequencies are not the quasi-decadal cycle for these six classes is an indication that the interaction between flooding and fire is affecting the vegetation dynamics differently than on other portions of the landscape.

A quasi-decadal signal has been recently noted (though not quantified) in flow velocity data for a few hydrography stations in the Okavango Delta (Wolski and Murray-Hudson, 2006). Since decadal oscillations have been observed in solar/climatic indices (Friis-Christensen and Lassen, 1991; Hurrell, 1995; Wang and Wang, 1996), the quasi-decadal signal was added in a second iteration of the harmonic regression in order to remove any effects of the long-term cycle from the overall trend. The detection of a quasi-decadal signal in vegetative response from remotely sensed imagery indicates a new and exciting capability for linking trends and patterns (e.g., teleconnections) observed in ~~climate~~ ^ and oceanic data with vegetation in terrestrial ecosystems. The T-test and 2-tailed significance of each model coefficient (i.e., semi-annual, annual, and quasi-decadal terms) for each EVI cluster are listed in Table 3. Again, the annual cycle was statistically significant for all EVI clusters. The semi-annual cycle was statistically significant for all but three EVI clusters and the quasi-decadal signal was statistically significant for all but five EVI clusters. As discussed previously, a potential resilience indicator may be the direction and magnitude

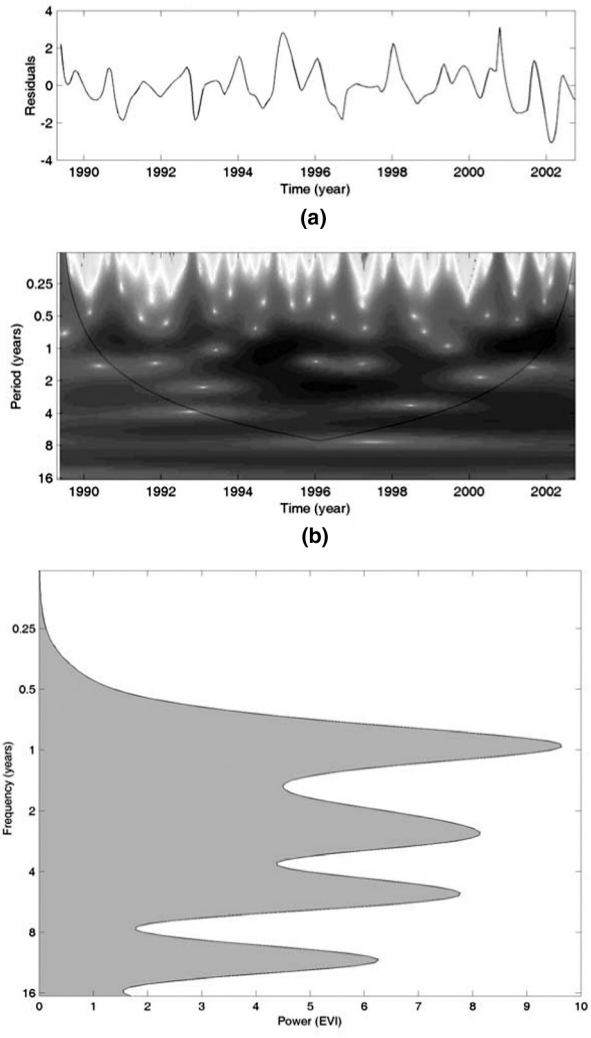

Figure 3. (a) Time-series of EVI residuals for Cluster 2, (b) Wavelet power spectrum for Cluster 2, and (c) Global wavelet for EVI-cluster 2 residual trajectory. Dominant frequencies identified from wavelet analysis include 1-year, 2.6-years, 5.1-years, and 10.9-years.

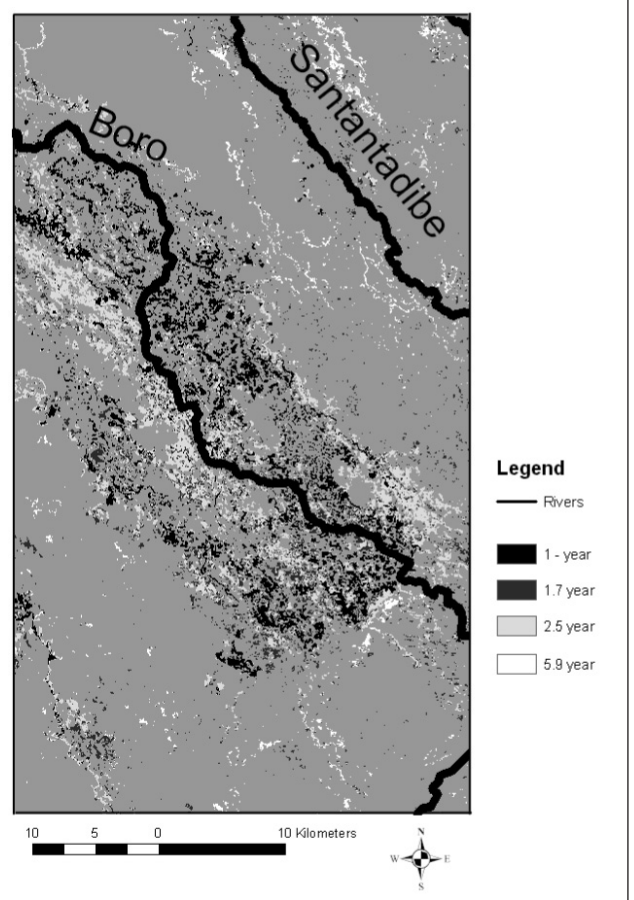

Figure 4. Shaded pixels indicate portions of the Distal Okavango where the dominant residual frequency was either 1-year, 1.7-years, 2.5-years, or 5.9-years.

(i.e., general trend) of the vegetation signal (Table 4). The trend results indicate four general directions in EVI change over time: strong positive ($+10^{-5}$), positive ($+10^{-6}$), no trend ($+/-10^{-7}$), and negative trend (-10^{-6}) (Figure 5). While the trend values are small, the direction and relative magnitude provide an interesting perspective regarding the dynamics of this landscape and their spatial distribution on the landscape. Clusters having a strong positive trend tended to occur in the active floodplain, whereas clusters having a negative trend appeared to be proximate to Maun and other settlements within the study area. Clusters having a positive trend or no trend were associated with woodlands as well as with savannas not located near settlements.

The variability in the vegetation response appears to be both largely cyclical and well defined by the semi-annual, annual, and quasi-decadal fits: 63 to 88 percent of the variance was explained using this simple harmonic model (Figure 6). Generally, clusters that fell within the floodplains but were only occasionally flooded, or regions that were frequently burned, were less well predicted by the harmonic regression. Those lower R^2 values can be attributed to influences not represented in this phase of the research, such as anthropogenic factors as well as changes or anomalies to the natural regimes. For example, EVI clusters 2, 3, and 4 are floodplain/wetland classes that did not experience flooding during the mid-1990s. This disruption to the annual flooding regime likely resulted in the poorer overall fit. In contrast, clusters that were consistently flooded or were less susceptible to burning resulted in the highest overall R^2.

Comparison of Transitory Signals to Disturbance and Landscape Stratification

As defined previously, a transitory signal relates to temporary dynamics resulting from a non-recurring event, such as disturbance. The transitory signal was represented as the residual from the semi-annual, annual, and quasi-decadal regression fit from the EVI-based trajectories. To determine the relationship, if any, of disturbance on vegetation productivity as detected using remotely sensed EVI, the pairwise correlations at the 0^{th} lag between the transitory signals and the flooding and fire trajectories of each class were computed (Table 5). Although ten of the correlation values between fire and the transitory signal were statistically significant, the correlation values themselves were quite low. Overall, little

TABLE 3. TWO-TAILED T-TEST AND SIGNIFICANCE OF EACH MODEL COEFFICIENT TERM (SEMI-ANNUAL, ANNUAL, AND QUASI-DECADAL) FOR ALL 35 EVI CLUSTERS. ~~SIGNIFICANT COEFFICIENTS ARE HIGHLIGHTED IN GREY~~

EVI Cluster	Semi-Annual		Annual		Decadal	
	T-test	*p*	T-test	*p*	T-test	*p*
1	−1.96	0.0268	15.31	<0.0001	−1.21	0.1150
2	−1.55	0.0626	10.57	<0.0001	−0.62	0.2692
3	1.52	0.0063	99.79	<0.0001	−2.43	0.0087
4	0.98	0.1663	10.40	<0.0001	0.79	0.2157
5	2.21	0.015	14.84	<0.0001	−2.67	0.0046
6	2.21	0.015	20.62	<0.0001	−3.27	0.0008
7	1.80	0.0365	16.58	<0.0001	−5.40	<0.0001
8	3.41	0.0005	11.58	<0.0001	−0.47	0.3198
9	2.69	0.0044	14.14	<0.0001	−2.51	0.0071
10	−3.41	0.0005	12.27	<0.0001	−2.35	0.0107
11	−4.11	<0.0001	15.12	<0.0001	2.18	0.0162
12	−6.22	<0.0001	17.66	<0.0001	−1.23	0.1112
13	−4.17	<0.0001	12.84	<0.0001	−2.71	0.0041
14	5.17	<0.0001	17.87	<0.0001	−2.41	0.0092
15	5.21	<0.0001	12.41	<0.0001	−2.69	0.0044
16	−4.23	<0.0001	13.12	<0.0001	−3.08	0.0014
17	5.21	<0.0001	14.49	<0.0001	−1.96	0.0268
18	4.50	<0.0001	14.62	<0.0001	−3.10	0.0014
19	6.22	<0.0001	17.85	<0.0001	−2.76	0.0036
20	6.26	<0.0001	16.98	<0.0001	−2.85	0.0028
21	−3.35	<0.0001	14.71	<0.0001	−3.24	0.0009
22	4.36	<0.0001	17.91	<0.0001	−3.19	0.0010
23	5.01	<0.0001	17.39	<0.0001	−3.41	0.0005
24	4.70	<0.0001	17.62	<0.0001	−3.33	0.0007
25	−2.79	0.0033	15.23	<0.0001	−4.87	<0.0001
26	−4.55	<0.0001	16.19	<0.0001	−4.24	<0.0001
27	−4.60	<0.0001	16.31	<0.0001	−4.45	<0.0001
28	−4.22	<0.0001	14.72	<0.0001	−3.78	0.0002
29	3.99	0.0001	19.33	<0.0001	−3.50	0.0004
30	−5.06	<0.0001	16.65	<0.0001	−2.91	0.0024
31	5.08	<0.0001	15.23	<0.0001	−3.12	0.0013
32	−3.78	0.0002	16.08	<0.0001	−4.03	<0.0001
33	1.23	0.1112	15.43	<0.0001	−5.42	<0.0001
34	4.19	<0.0001	18.84	<0.0001	−3.65	0.0002
35	4.09	<0.0001	20.16	<0.0001	−3.65	0.0002

evidence of strong correlation between flooding, fire, and transitory signals was revealed. Limitations of the correlation analysis between the transitory signal and the observed flooding and fire regimes include weak signals that may not be observable and a non-uniform image acquisition. It is also possible that the 35 ISODATA-based temporal clusters obscured vegetation changes related to more local-scaled processes, such as microclimatic conditions or management strategies.

TABLE 4. GENERAL TREND OF EVI-BASED TRAJECTORY CLASSES AND THE R^2 OF A SEMI-ANNUAL, ANNUAL FIT, AND QUASI-DECADAL FIT

EVI Cluster	Trend	R^2	EVI Cluster	Trend	R^2
1	1.06E-05	0.7880	19	−3.93E-06	0.8479
2	1.01E-05	0.6714	20	−3.49E-06	0.8497
3	1.17E-05	0.6893	21	8.13E-06	0.8149
4	7.29E-06	0.6258	22	1.23E-06	0.8109
5	1.11E-05	0.7806	23	−4.92E-07	0.8468
6	6.12E-06	0.8633	24	1.25E-06	0.8176
7	1.51E-05	0.8460	25	−1.66E-06	0.7850
8	8.44E-06	0.6773	26	−1.44E-06	0.8109
9	7.67E-06	0.7736	27	2.43E-06	0.8141
10	7.02E-06	0.7549	28	−1.89E-06	0.7817
11	2.24E-06	0.7525	29	5.66E-06	0.8675
12	8.23E-07	0.8318	30	−4.38E-06	0.8533
13	−3.31E-06	0.7183	31	−2.32E-06	0.8261
14	−2.53E-06	0.8024	32	5.83E-06	0.8329
15	−3.12E-06	0.7528	33	1.41E-05	0.8160
16	−3.58E-06	0.7522	34	2.39E-06	0.8711
17	−3.77E-06	0.7660	35	5.58E-06	0.8810
18	9.23E-07	0.7533			

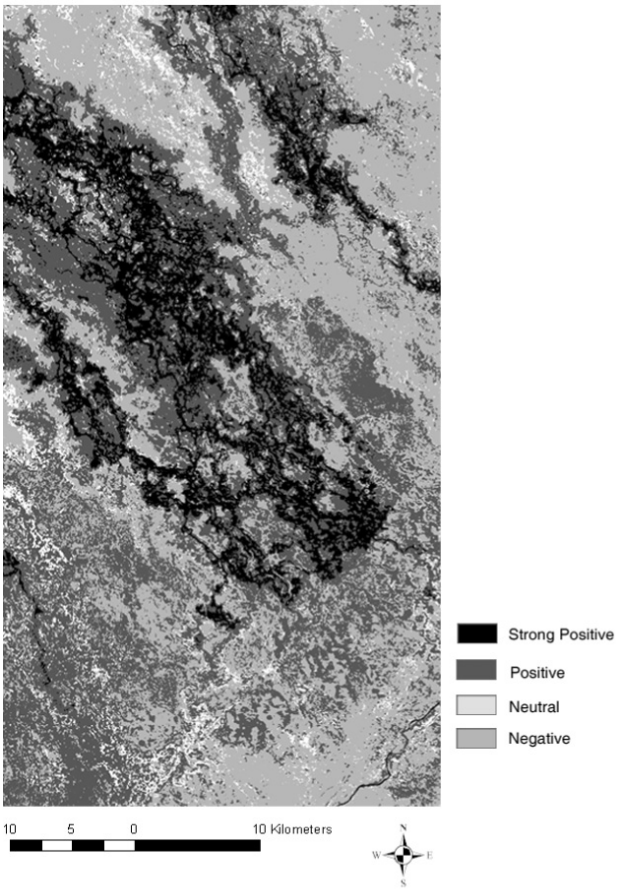

Figure 5. Shaded areas indicate portions of the landscape associated with different secular change of EVI values during 1989 to 2002. Black indicates strong positive trend ($+10e^{-5}$), Dark Grey indicates positive trend ($+10e^{-6}$), Light Grey indicates no trend, and Medium Grey indicates negative trend ($-10e^{-6}$).

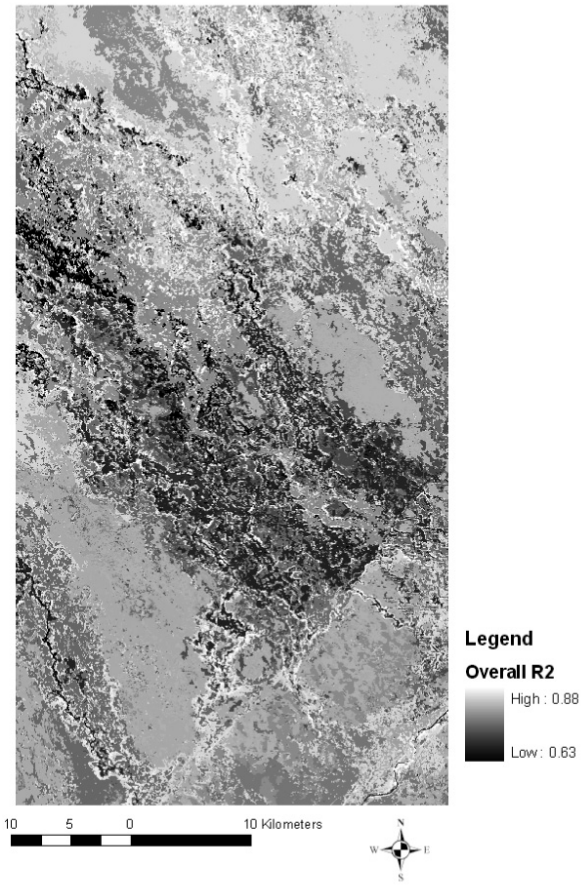

Figure 6. Overall R^2 of semi-annual, annual, and quasi-decadal regression fit on 35 EVI-based clusters in the study area.

In order to further refine the results, it was deemed necessary to assess the impact of anthropogenic factors and land management on the landscape by repeating the above analysis under two new scenarios that accounted for urban/agricultural impacts and landscape management regimes respectively. First, the Maun village area and agricultural fields were masked via heads-up interpretation and digitizing from a pan-sharpened 2003 September ALI image, in consultation with GPS field data on land-use collected in 2001 and 2006. The masked ~~regions of urban and agriculture~~ were subsequently assigned to additional classes (36 and 37, respectively). Agricultural fields were operationalized as geometric plots spectrally different than the rest of the natural landscape; the urban extent was primarily based upon settlement density.

While the recomputed general trend and R^2 of the semi-annual, annual and quasi-decadal fit for nearly all of the trajectories exhibited similar trends as in the 35-cluster analysis (Table 6), the urban class (class 36) demonstrated a negative trend of equivalent magnitude with the other negative-trending classes. The agriculture class (class 37), however, had a negative trend approximately double all the other classes. One possible explanation for this decrease in EVI relates to the observation of woody (Acacia and Mopane) encroachment in several of these areas visited in May 2006 and May 2007, since these associations tend to exhibit lower EVI responses than many herbacious associations. However, without data on grazing usage, further speculation would be premature given the proximity of this area to settlements and its location primarily within communal/open access lands. For the second [management regime] scenario, lands designated as belonging to the Moremi Game Reserve, photographic concessions, hunting concessions, or communal /open access regions were stratified with boundary files and EVI-trajectories computed for each of the four management types (Figure 7). The general trend and the R^2 of the semi-annual, annual and quasi-decadal fits for the aggregated analysis under the land management masks (Table 7) were not revealing as the variability of the vegetation within each mask confounds the discernibility of the more subtle impacts. In contrast, visual inspection of the 35 EVI-clusters trend change revealed that much of the negative trending vegetation occurred in the communal and photographic concessions. However, the hunting concession (including the more frequently burned floodplains) and the communal areas were more poorly fit with the harmonic regression.

Conclusions

Our results reveal new possibilities in the way remotely sensed imagery is utilized to assess vegetation response as a function of predicted climatic patterns and disturbance.

Table 5. Correlations and Significance Between Transitory Signals from EVI Cluster Trajectories and Flooding and Fire Trajectories as well as Between Flooding and Fire. Correlations with a Statistical Significance Better than 0.05 are Highlighted in Grey

EVI Cluster	Fire/Transitory		Flood/Transitory		Fire/Flood	
	R	*p*	R	*p*	R	*p*
1	0.2485	0.0232	−0.0127	0.9089	−0.3161	0.0032
2	−0.0229	0.8362	0.1034	0.3492	−0.2219	0.0413
3	0.1827	0.0962	−0.0236	0.8309	−0.2280	0.0358
4	−0.0365	0.7418	0.1397	0.2051	−0.1824	0.0948
5	0.3693	0.0005	−0.0691	0.5322	−0.1976	0.0699
6	0.2514	0.0211	0.0289	0.7939	−0.0430	0.6960
7	0.4483	<0.0001	0.0965	0.3826	0.1230	0.2620
8	−0.0048	0.9656	0.3477	0.0012	−0.0764	0.4869
9	0.2959	0.0063	0.0431	0.6969	−0.1111	0.3115
10	0.0126	0.9098	0.1021	0.3555	−0.0690	0.5304
11	0.1975	0.0718	0.1043	0.3453	−0.0230	0.8343
12	0.0717	0.5166	0.2092	0.0561	−0.0820	0.4557
13	0.2196	0.0447	0.0917	0.4070	0.1036	0.3454
14	0.1199	0.2773	0.0139	0.9004	0.2953	0.0061
15	0.2053	0.0611	0.0443	0.6890	0.2289	0.0351
16	0.2123	0.0525	0.0515	0.6417	−0.0003	0.9979
17	0.1128	0.3070	0.0670	0.5448	−0.0250	0.8201
18	0.0814	0.4614	0.0491	0.6571	−0.0186	0.8658
19	0.1365	0.2156	−0.0413	0.7092	0.4395	<0.0001
20	0.1148	0.2985	−0.0706	0.5233	0.0708	0.5196
21	0.2185	0.0458	−0.0995	0.3679	−0.0442	0.6881
22	0.1185	0.2832	0.0120	0.9136	0.3789	0.0003
23	0.1114	0.3131	0.0866	0.4336	0.1254	0.2528
24	0.0682	0.5376	−0.1201	0.2764	0.1255	0.2524
25	0.0298	0.7878	0.0359	0.7460	0.2887	0.0074
26	0.0935	0.3975	−0.0319	0.7735	0.1118	0.3085
27	0.1365	0.2156	0.0253	0.8191	−0.0038	0.9724
28	0.1252	0.2565	0.1113	0.3137	0.2950	0.0061
29	0.2709	0.0127	0.1349	0.2212	0.3192	0.0029
30	0.1448	0.1889	0.1130	0.3062	0.0077	0.9442
31	0.0856	0.4386	−0.0550	0.9607	0.0690	0.5303
32	0.1203	0.2756	−0.0216	0.8455	−0.0337	0.7596
33	0.4454	<0.0001	0.1872	0.0881	0.3661	0.0006
34	0.0923	0.4035	0.0394	0.7220	0.0042	0.9699
35	0.1462	0.1845	0.1211	0.2727	0.1567	0.1520

Rather than using Fourier analysis to segment the landscape based upon identified periodicities (i.e., seasonality), a harmonic regression was employed to assess how well different portions of the landscape fit with periodicities reported in the climatic change and vegetation ecology literatures. The landscape within the study area was stratified using statistical clustering of the vegetation response through time and different land management practices to

Table 6. General Trend of evi-based Trajectory Classes Including Urban and Agriculture (Class 36 and 37, Respectively) and the R^2 of a Semi-annual, Annual, and Quasi-decadal Fit

Cluster	Trend	R^2	Cluster	Trend	R^2
1	1.08E-05	0.7967	20	−2.49E-06	0.7976
2	1.15E-05	0.6219	21	9.11E-06	0.7665
3	1.31E-05	0.6231	22	1.51E-06	0.8190
4	8.05E-06	0.6182	23	3.23E-07	0.8091
5	1.15E-05	0.7859	24	1.45E-06	0.8254
6	6.43E-06	0.8688	25	−1.21E-07	0.7856
7	1.54E-05	0.8506	26	−1.27E-06	0.8152
8	9.29E-06	0.6631	27	2.77E-06	0.8122
9	8.29E-06	0.7568	28	−1.31E-06	0.7691
10	8.27E-06	0.6890	29	6.31E-06	0.8447
11	2.65E-06	0.7584	30	−3.36E-06	0.7958
12	1.59E-06	0.8051	31	−1.00E-06	0.7629
13	−2.45E-06	0.6971	32	6.78E-06	0.7921
14	−1.97E-06	0.8161	33	1.45E-05	0.8205
15	−1.79E-07	0.6847	34	3.35E-06	0.8313
16	−2.52E-06	0.7106	35	6.37E-06	0.8535
17	−2.51E-06	0.7416	36	−3.49E-06	0.7714
18	1.56E-06	0.7507	37	−5.82E-06	0.7546
19	−3.10E-06	0.8160			

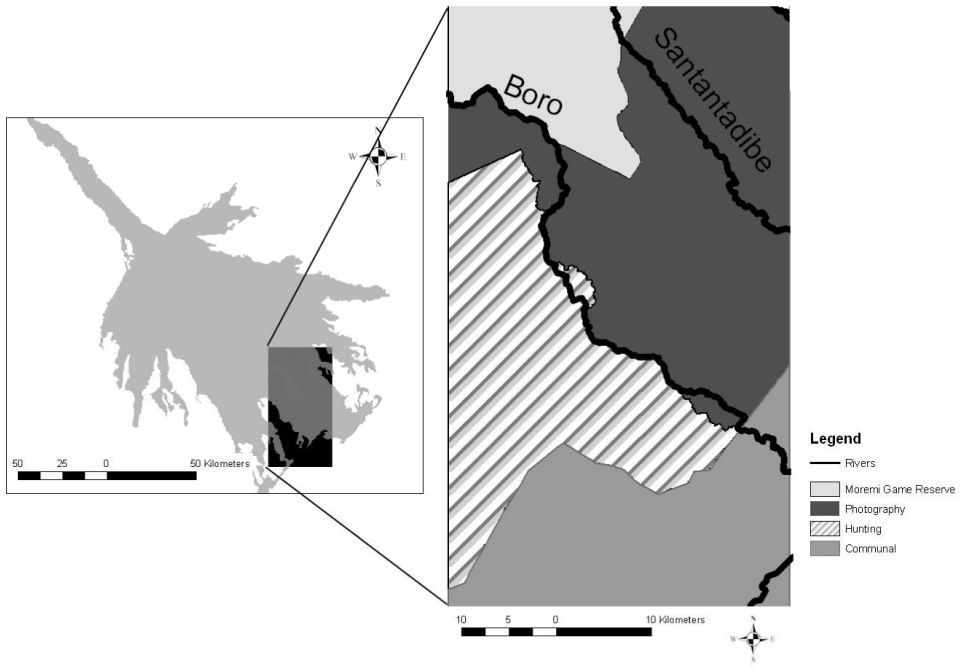

Figure 7. Land management designation and location of primary river channels in the Distal Okavango Delta.

assess spatio-temporal associations in EVI change. In the Okavango Delta, portions of the landscape that were found to fit well with climatic cycles include channels, reeds/sedges, riparian vegetation, and woodlands. In contrast, portions of the landscape that did not fit as well to detected climatic patterns include less frequently flooded floodplains as well as floodplains that were frequently burned. In general, higher R^2 values tended to be associated with classes experiencing lower levels of observed burning, experiencing higher levels of flooding, or existing outside the communal/open access areas.

The ability to quantify vegetation response to climatic patterns and disturbance using time-series analysis can be utilized to identify regions at risk or vulnerable to future climate or land-use change scenarios. As the results indicate, the seasonal, annual and quasi-decadal terms account for the majority of variance observed in the time-series. Furthermore, the residual signals also contain frequencies that may be a combination of climatic and anthropogenic effects. Subsequent analysis of the transitory signals shows that only ten of the EVI clusters' transitory signals were statistically correlated with fire; however the correlation values of each of the clusters were low. Similarly, flooding was not found to be correlated with the EVI transitory signals. This lack of correlation with the transitory signals suggests that, for systems where disturbances (here, specifically flooding and fire) are part of a regime (i.e., not a single stochastic event), the vegetation is likely adapted to these events and their presence does not affect or change the direction of the observed trajectories. Transitory signals, as described by Rodriguez-Arias and Rodo (2004), however, might be correlated with stochastic disturbances on a landscape, especially if the disturbance had a large spatial footprint.

TABLE 7. GENERAL TREND OF LAND MANAGEMENT EVI-BASED TRAJECTORY CLASSES AND THE R^2 OF A SEMI-ANNUAL, ANNUAL, AND QUASI-DECADAL FIT

	Trend	R^2
Moremi	1.52E-06	0.8210
Photo	3.49E-06	0.8273
Hunting	4.33E-06	0.7677
Communal	5.66E-07	0.7941

The utilization of multitemporal imagery for the development of resilience indicators also holds promise for future studies. In this research, floodplains that are affected by frequent burning or subject to drought were less well characterized by the harmonic regression. These areas could be considered as potentially influenced by disturbance and perhaps less resilient. Landscapes that are less resilient to disturbance such as drought, fire, grazing, or insect outbreak could experience dramatic shifts in the vegetation assemblages and ecosystem services. It remains to be seen whether these areas are less resilient than other regions in the study area, as even a fourteen-year time-series may be inadequate to capture the cycles and dynamics at work in such a complex mosaic (Rappaport *et al.*, 1998; Turner *et al.*, 2001). The utilization of time-series analysis on remotely sensed imagery in conjunction with *in situ* derived knowledge can be a powerful tool for mapping and monitoring vegetation response to anthropogenic and climate change (Kerr and Ostrovsky, 2003).

The analysis of the EVI-residual trajectories indicated a quasi-decadal signal which is potentially out of phase with general 8-, 18-, and 80-year precipitation cycles reported for Southern Africa by Tyson et al. (2002), yet agrees with periodicities observed in precipitation data collected at the Maun airport. However, part of further testing the relationship of local land-use and vegetation fluctuations against more regionalized forcing factors necessarily entails refining the assessment of mitigating anthropogenic factors that may be impacted by local and/or regional factors. Here,

in particular, the land management zones correspond fairly strongly to temporal flooding zones and floodplain position. As such, further work disentangling this potentially confounding effect is required. Further, we quantitatively assessed the vegetation trajectories by separable temporal clusters and by management zones, but testing the interactions of the two may provide more nuanced results.

This research provides a methodology for quantifying differential vegetation response at the landscape level influenced by both climatic and anthropogenic forcing factors. This work extends methods previously developed for coarser spatial resolution datasets such as MODIS and AVHRR (Andres *et al.*, 1994; Moulin *et al.*, 1997; Moody and Johnson, 2001) to higher spatial resolution imagery (Landsat TM/ETM+) due to the depth of time-series available. Monitoring at a finer landscape level improves previous efforts unable to adequately capture the spatial heterogeneity inherent in this savanna/wetland system. The creation and analysis of a seasonally rich TM/ETM+ multi-temporal dataset may not always be practical or even possible, and as such the verification of when such an endeavor is required will help inform future studies as to data acquisition, preprocessing, and analysis choices. However, this approach is generalizable to other sensor systems. Further, the fusing of such medium resolution data with time-series signals derived from AVHRR/MODIS could provide one alternative to establishing an operational monitoring approach applicable for multiscale regional monitoring, modeling, mapping, and management efforts.

Acknowledgments

This work was supported by NASA Earth Systems Science Fellowship No. NNG04GR09H, NSF Doctoral Dissertation Research Improvement Grant No. BCS-0503178, and by the following sources at The University of Texas at Austin: Vice President for Research, College of Liberal Arts, David and Mary Miller Continuing Fellowship, and Veselka Travel Award (Department of Geography and the Environment). Data were provided by the NASA Safari 2000 Mission, NASA EO-1 Scientific Calibration/Validation Mission, Techniche Universitaet Muenchen, and the Harry Oppenheimer Okavango Research Centre of the University of Botswana (Maun).

References

Andersson, L., T. Gumbricht, D. Hughes, D. Kniveton, S. Ringrose, H. Savenije, M. Todd, J. Wilka, and P. Wolski, 2003. Water flow dynamics in the Okavango River Basin and Delta -A prerequisite for the ecosystems of the delta, *Physics and Chemistry of the Earth, Parts A/B/C* 28(20–27):1165–1172

Andres, L., W.A. Salas, and D.L. Skole, 1994. Fourier analysis of multitemporal AVHRR data applied to a land cover classification, *International Journal of Remote Sensing*, 15:1115–1121.

Ashton, P., 2003. The search for an equitable basis for water sharing in the Okavango River basin, *International Waters in Southern Africa* (M. Nakayama, editor), United Nations University Press, New York, pp. 164–188.

Bennett, E.M., G.S. Cumming, and G.D. Peterson, 2005. A systems model approach to determining resilience surrogates for case studies, *Ecosystems*, 8:945–957.

Bradley, B.A., R.W. Jacob, J.F. Hermance, and J.F. Mustard, 2007. A curve fitting procedure to derive interannual phenologies from time series of noisy satellite NDVI data, *Remote Sensing of Environment*, 106(2):137–145.

Braswell, B.H., D.S. Schimel, E. Linder, and B. Moore III, 1997. The response of global terrestrial ecosystems to interannual temperature variability, *Science*, 278:870–873.

Chavez, P., and D.J. MacKinnon, 1994. Automatic detection of vegetation changes in the southwestern United States using remotely sensed images, *Photogrammetric Engineering & Remote Sensing*, 60(5):567–585.

Chavez, P.S., 1988. An improved dark-object subtraction technique for atmospheric scattering of multispectral data, *Remote Sensing of Environment*, 24(3):459–479.

Crews-Meyer, K.A., 2002. Characterizing landscape dynamism via paneled-pattern metrics, *Photogrammetric Engineering & Remote Sensing*, 68(10):1031–1040.

DeAngelis, D.L., and J.C. Waterhouse, 1987. Equilibrium and nonequilibrium concepts in ecological models, *Ecological Monographs*, 57:1–21

Ellery, W.N., T.S. McCarthy, and N.D. Smith, 2003. Vegetation, hydrology, and sedimentation patterns on the major distributary systems of the Okavango Fan, Botswana, *Wetlands*, 23(2):357–375.

Fang, H., S. Liang, M.P. McClaran, W.J.D. van Leeuwen, S. Drake, S.E. Marsh, A.M. Thomson, R.C. Izaurralde, and N.J. Rosenberg, 2005. Biophysical characterization and management effects on semiarid rangeland observed from Landsat ETM+ data, *IEEE Transactions on Geoscience and Remote Sensing*, 42(1):125–134.

Ferreira, L.G., H. Yoshioka, A. Huete, and E.E. Sano, 2003. Seasonal landscape and spectral vegetation index dynamics in the Brazilian Cerrado: An analysis within the large-scale biosphere-atmosphere experiment in Amazonia (LBA), *Remote Sensing of Environment*, 87:534–550.

Folke, C., S. Carpenter, B. Walker, M. Scheffer, T. Elmqvist, L. Gunderson, and C.S. Holling, 2004. Regime shifts, resilience, and biodiversity in ecosystem management, *Annual Review of Ecology, Evolution, and Systematics*, 35:557–581.

Friis-Christensen, E., and K. Lassen, 1991. Length of the solar cycle: An indicator of solar activity closely associated with climate, *Science*, 254(5032):698–700.

Gao, X., A. Heute, W. Ni, and T. Miura, 2000. Optical-biophysical relationships of vegetation spectra without background contamination, *Remote Sensing of Environment*, 74:609–620.

Heinl, M., A.L. Neuenschwander, and J. Silva, 2006. Interactions between fire and flooding in a southern African floodplain (Okavango Delta, Botswana), *Landscape Ecology*, 21(5):699–709.

Holling, C.S., 1973. Resilience and stability of ecological systems, *Annual Review of Ecology and Systematics*, 4:1–23.

Huete, A.R., K. Didan, T. Miura, E.P. Rodriguez, X. Gao, and L.G. Ferriera, 2002. Overview of the radiometric and biophysical performance of the MODIS vegetation indices, *Remote Sensing of Environment*, 83:195–213.

Huete, A.R., H.Q. Liu, K. Batchily, and W. van Leeuwen, 1997. A comparison of vegetation indices over a global set of TM images, *Remote Sensing of Environment*, 59:440–451.

Hurrell, J., 1995. Decadal trends in the North Atlantic oscillation: Regional temperatures and precipitation, *Science*, 269(5224):676–679.

Jassby, A.D., and T.M. Powell, 1990. Detecting changes in ecological time series, *Ecology*, 71(6):2044–2052.

Kerr, J.T., and M. Ostrovsky, 2003. From space to species: Ecological applications for remote sensing, *Trends in Ecology & Evolution*, 18(6):299–305.

Kestin, T.S., D.J. Karoly, J. Yano, and N.A. Rayner, 1998. Time-frequency variability of ENSO and stochastic simulations, *Journal of Climate*, 11:2258–2272.

Kgathi, D.L., D. Kniveton, S. Ringrose, A.R. Turton, C. Vanderpost, J. Lundqvist, and M. Seely, 2006. The Okavango: A river supporting its people, environment and economic development, *Journal of Hydrology*, 331(1/2):3–17.

Kgathi, D.L., G. Mmopelwa, and K. Mosepele, 2005. Natural resources assessment in the Okavango Delta, Botswana: Case studies of key resources, *Natural Resources Forum*, 29:70–81.

Labat, E., J. Ronchail, J. Callede, J.L. Guyot, E. De Oliveira, and W. Guimaraes, 2004. Wavelet analysis of the Amazon hydrological regime variability, *Geophysical Research Letters*, 31:L02501, doi:10.1029/2003GL018741.

Lundberg, P., E. Ranta, J. Ripa, and V. Kaitala, 2000. Population variability in space and time, *Trends in Ecology and Evolution*, 15(11):460–464.

Mbaiwa, J.E., F.E. Bernard, and C.E. Orford, 2002. Limits of acceptable change for tourism in the Okavango Delta, *Proceedings of the Conference on Environmental Monitoring of Tropical and Subtropical Wetlands, Maun, Botswana*, URL: http://www.globalwetlands.org (last date accessed: 10 February 2008).

McCarthy, J., T. Gumbricht, and T.S. McCarthy, 2006. Ecoregion classification in the Okavango Delta, Botswana from multitemporal remote sensing, *International Journal of Remote Sensing*: *Remote Sensing, NASA/Safari 2000 Special Issue*, 26(19):4339–4357.

McCarthy, T.S., G.R.J. Cooper, P.D. Tyson, and W.N. Ellery, 2000. Seasonal flooding in the Okavango Delta, Botswana – Recent history and future prospects, *South African Journal of Scienc*e, 96:25–33.

McCarthy, T.S., W.N. Ellery, and A. Bloem, 1998. Some observations on the geomorphological impact of hippopotamus *(Hippopotamus amphibius* L.) in the Okavango Delta, Botswana, *African Journal of Ecology*, 36:44–56.

Mi, X., H. Ren, Z. Ouyang, W. Wei, and K. Ma, 2005. The use of the Mexican Hat and the Morlet wavelets for detection of ecological patterns, *Plant Ecology*, 179:1–19.

Moody, A., and D.M. Johnson, 2001. Land-surface phenologies from AVHRR using the discrete fourier transform, *Remote Sensing of Environment*, 75:305–323.

Moulin, S., L. Kergoat, N. Viovy, and G. Dedieu, 1997. Global scale assessment of vegetation phenology using NOAA/AVHRR satellite measurements, *Journal of Climate*, 10(6):1154–1170.

Neuenschwander, A.L., and K.A. Crews-Meyer, 2006. Multitemporal mapping of disturbances in the Okavango Delta, Botswana using Landsat TM and ETM+ data, *Proceedings of the 2006 IGARRS Conference*, Denver, Colorado.

Neuenschwander, A.L., M.M. Crawford, and S. Ringrose, 2006. Results of the EO-1 experiment: Use of Earth Observing-1 Advanced Land Imager (ALI) data to assess the vegetational response to flooding in the Okavango Delta, Botswana, *International Journal of Remote Sensing*: *Remote Sensing, NASA/Safari 2000 Special Issue*, 26(19):4321–4337.

Rappaport, D.J., R. Costanza, and A.J. McMichael, 1998. Assessing ecosystem health, *Trends in Ecology and Evolution*, 13:397–402.

Rodriguez-Arias, M.A., and X. Rodo, 2004. A primer on the study of transitory dynamics in ecological series using the scale-dependent correlation analysis, *Oecologica*, 138:485–504.

Rodriguez-Trelles, F., G. Alvarez, and C. Zapata, 1996. Time-series analysis of seasonal changes in the O inversion polymorphism of Drosophila subobscura, *Genetics*, 142:179–187.

Saunders, S.C., J. Chen, T.D. Drummer, E.J. Gustafson, and K.D. Brosofske, 2004. Identifying scales of pattern in ecological data: A comparison of lacunarity, spectral and wavelet analysis, *Ecological Complexity*, 2:87–105.

Schroeder, T.A., W.B. Cohen, C. Song, M.J. Canty, and Z. Yang, 2006. Radiometric correction of multi-temporal Landsat data for characterization of early successional forest patterns in western Oregon, *Remote Sensing of Environment*, 103:16–26.

Song, C., C.E. Woodcock, K.C. Seto, M. Pax-Lenney, and S.A. Macomber, 2001. Classification and change detection using Landsat TM data: When and how to correct atmospheric effects, *Remote Sensing of Environment*, 75:230–244.

Torrence, C., and G.P. Compo, 1998. A practical guide to wavelet analysis, *Bulletin of the American Meteorological Society*, 79(1):61–78.

Turner, M.G., R.H. Gardner, and R.V. O'Neill, 2001. *Landscape Ecology in Theory and Practice: Pattern and Process*, Springer Press, New York.

Tyson, P.D., G.R.J. Cooper, and T.S. McCarthy, 2002. Millennial to multi-decadal variability in the climate of southern Africa, *International Journal of Climatology*, 22:1105–1117.

Wang, B., and Y. Wang, 1996. Temporal structure of the Southern Oscillation as revealed by waveform and wavelet analysis, *Journal of Climate*, 9:1586–1598.

West, M., 1997. Time series decomposition, *Biometrika*, 84(2):489–494.

Wolski, P., and M. Murray-Hudson, 2006. Flooding dynamics in a large low-gradient alluvial fan, the Okavango Delta, Botswana, from analysis and interpretation of a 30 year hydrometric record, *Hydrology and Earth System Sciences*, 10:127–137.